2.26 to 2.46 GHz. Hence, the antennas electrical length increases. Therefore, w_R is only suppressed as it is not affected by L_L.

Figure 7 shows the surface current distribution at 2.26 and 2.89 GHz. There is a strong surface loop current flowing mainly between the TL and the second unit cell. This shows dependence of the resonance frequency on the shunt inductance L_L and capacitive gaps C_L. While at 2.89 GHz, out-of-phase currents flows in the two stubs which excite resonance frequency at 2.89 GHz. Figures 8 shows simulated radiation efficiency and peak realized gain. The simulated radiation efficiency of the proposed antenna at 2.26 GHz is 64% and 92% at 2.89 GHz. The realized gain is 1.74 dBi at 2.26 GHz and 2.69 dBi at 2.89 GHz. Table 1 shows the comparison of the gains and efficiency of the proposed antenna with the reference antennas. Figures 9 and 10 show simulated and measured radiation patterns. Due to the shift in the resonance frequencies of the fabricated prototype, the measurement is carried out at 2.25 and 2.98 GHz. There is close resemblance between the measured and simulated radiation patterns obtained for both *E*-plane and *H*-planes. A bidirectional radiation patterns are obtained in the *E*-plane and omnidirectional patterns in *H*-planes.

5. CONCLUSION

A dual-band CRLH metamaterial antenna has been proposed in this article. The antenna was composed of two planar CRLH unit cells with compact dimensions of 31 mm × 22 mm × 1.57 mm (0.23 λ_o × 0.17 λ_o × 0.011 λ_o) at 2.26 GHz. The dispersion diagram shows the resonance characteristics of the unit cell. The resonance frequency of the negative order mode is controlled by the circulating loop currents, and multiband characteristics can be achieved by increasing the number of unit cells. The dual-band prototype is fabricated and measured with peak realized gains of 1.74 and 2.69 dBi at 2.26 and 2.89 GHz, respectively. And a peak radiation efficiency of 92% was obtained for a frequency range of 2–3 GHz.

REFERENCES

1. A. Lai, T. Itoh, and C. Caloz, Composite right/left-handed transmission line metamaterials, IEEE Microwave Mag 5 (2004), 34–50.
2. J.Y. Chin, J.N. Gollub, J.J. Mock, R. Liu, C. Harrison, D.R. Smith, and T.J. Cui, An efficient broadband metamaterial wave retarder, Opt Express 17 (2009), 7640–7647.
3. G.V. Eleftheriades, A.K. Iyer, and P.C. Kremer, Planar negative refractive index media using periodically L—C loaded transmission lines, IEEE Trans Microwave Theory Tech 50 (2002), 2702–2712.
4. B. Wu, W. Wang, J. Pacheco, X. Chen, T. Grzegorczyk, J.A. Kong, and P. Art, A study of using metamaterials as antenna substrate to enhance gain, Prog Electromagn Res 51 (2005), 295–328.
5. S. Kim, H.K. Choi, J.I. Choi, and J.H. Park, A new approach to the design of a dual-band IFA with a metamaterial unit cell, Microwave Opt Technol Lett 54 (2012), 545–549.
6. H.-Z. Yu and Q.-X. Chu, A broadband PIFA with zeroth-order resonators loading, Prog Electromagn Res Lett 21 (2011), 67–77.
7. A. Sanada, K. Masao, A. Ikuo, C. Caloz, and T. Itoh, A planar zeroth-order resonator antenna using a left-handed transmission line, In: 34th Europen Microwave Conference, Amsterdam, Holland, 2004, pp. 1341–1344.
8. S. Mok, S. Kahng, and Y. Kim, A wide band metamaterial ZOR antenna of a patch coupled to a ring mushroom, J Electromagn Waves Appl 26 (2012), 1667–1674.
9. H.A. Majid, M.K.A. Rahim, and T. Masri, Microstrip antenna's gain enhancement using left-handed metamaterial structure, Prog Electromagn Res 8 (2009), 235–247.
10. A. Lai, K.M.K.H. Leong, and T. Itoh, Infinite wavelength resonant antennas with monopolar radiation pattern based on periodic structures, IEEE Trans Antennas Propag 55 (2007), 868–876.
11. H.E.A. El-raouf and S.S. Zaheer, Design of small planar antennas based on double-layered CRLH metamaterials, Microwave Opt Technol Lett 54 (2012), 2224–2229.
12. T. Jang, J. Choi, and S. Lim, Compact coplanar waveguide (CPW)-Fed zeroth-order resonant antennas with extended bandwidth and high efficiency on vialess single layer, IEEE Trans Antennas Propag 59 (2011), 363–372.
13. A. Anghel and R. Cacoveanu, Improved composite right/left-handed cell for Leaky-wave antenna, Prog Electromagn Res Lett 22 (2011), 59–69.
14. S.-X. Liu and Q.-Y. Feng, Compact muti-band loop antennas using CPW-based CRLH Quarter-wave type resonators, Prog Electromagn Res C 28 (2012), 47–60.
15. F. Qureshi, M.A. Antoniades, and G.V Eleftheriades, A compact and low-profile metamaterial ring antenna with vertical polarization, IEEE Antennas Wireless Propag Lett 4 (2005), 333–336.
16. J. Choi and S. Lim, Frequency and radiation pattern reconfigurable small metamaterial antenna using its extraordinary zeroth-order resonance, J Electromagn Waves Appl 24 (2010), 2119–2127.
17. Y. Li and Q. Feng, A compact composite right-/left-handed transmission line antenna with extended bandwidth J Electromagn Waves Appl 27 (2012), 123–130.

© 2014 Wiley Periodicals, Inc.

DESIGN OF A PLANAR WIDEBAND PATCH ANTENNA FOR UHF RFID TAG

Mohd Saiful Riza Bashri, Muhammad Ibn Ibrahimy, and S. M. A Motakabber
Department of Electrical and Computer Engineering, International Islamic University Malaysia (IIUM), 53100 Kuala Lumpur, Malaysia; Corresponding author: ibrahimy@iium.edu.my

Received 8 November 2013

ABSTRACT: *In this article, a planar wideband microstrip patch antenna for ultrahigh frequency (UHF) radio identification (RFID) tag is presented. By incorporating two resonating C-shape patches, two resonances are excited close to each other to create wide impedance bandwidth to cover the entire operating frequency of UHF RFID system between 860 and 960 MHz for universal metal mountable tag. For complex impedance matching between the antenna input terminal and the referenced microchip whose impedance is $Z_{chip} = (31 - j212)$ Ω, a small rectangular loop feed structure was utilized where both of the resonating patches are magnetically coupled. The antenna design and simulation were carried out using finite element method based software, Ansoft HFSS v13. The simulated and measured radiation patterns at operating frequency of 915 MHz are in good agreement. The simulated and measured impedance bandwidth (Return Loss ≥ 3 dB) of 159 and 155 MHz were obtained that are well above the required 100 MHz bandwidth.* © 2014 Wiley Periodicals, Inc. Microwave Opt Technol Lett 56:1579–1584, 2014; View this article online at wileyonlinelibrary.com. DOI 10.1002/mop.28389

Key words: *complex impedance matching; patch antenna; radio frequency identification; metal object*

1. INTRODUCTION

Radio identification (RFID) technology has been adopted in many sectors such as supply chain management, object monitoring and tracking, access control to name a few [1, 2]. This pervasive and ubiquitous implementation of RFID system is due to several advantages offered by the technology like it does not require line of sight to operate, able to read several tags simultaneously, uniquely identify an object and can hold large information about the product compared to other automatic

identification (Auto-ID) technology such as barcode. A basic RFID system is comprised of a tag or multiple of tags and a reader [3]. Tag is a small wireless device to be attached to an object to be tracked and monitored while reader acts to read the information carried by the tag when the tagged objects are within the vicinity of the reader.

RFID system can be classified into several categories based on the operating frequency, power source, and protocols that govern its communication. Low frequency (LF), high frequency (HF), ultrahigh frequency (UHF), and microwave are the main operating frequency band of RFID system. LF and HF systems operate in the near field region via inductive coupling between the tag and reader's coils while UHF and microwave system communicate in the far field region through the traveling electromagnetic wave [4]. As a result, UHF system hold several advantages over other systems like longer read range, higher transmission rate, and larger storage capacity. Due to these factors, UHF system is rapidly becoming the preferred solutions in most of today's RFID applications. Conversely, tag can be grouped into three main categories which are active tag, semiactive tag, and passive tag. This classification is made based on how the tag microchip is powered up to operate. Unlike passive tag, active tag is equipped with internal power source such as battery or energy harvested circuit and transmitter. Meanwhile, semiactive tag has its own internal power source but in the absence of transmitter. For passive and semiactive tag, due to the absence of transmitter, the communication from the tag to the reader is performed using a unique modulation technique called back-scattering modulation [5]. The modulation is executed by the microchip by changing its front end complex RF input impedance to match and mismatch with the impedance at the tag antenna input terminal. This match and mismatch states corresponds to the bit "0" and "1," respectively. The resulting reflected power received by the reader varies between two states high and low, thus enable the demodulation of the information sent by the tag. The operating frequency of each country varies within the UHF band. In European region, the allocated frequency band is 866–868 MHz, in North America, 902–928 MHz is utilized, whereas 952–956 MHz is the frequency band used in Japan [6]. Typical configuration of tag is shown in Figure 1. To successfully implement RFID system, several factors need to be considered like cost, read range, reliability, and size. The cost of tag can be significantly reduced by adopting a passive system and is the main interest of this research.

In passive UHF RFID system, tag antenna plays a pivotal role to ensure the system is able to meet the requirements. The most common type of antenna used is label-type modified dipole antenna. This type of antenna is adopted mainly due its low cost, thin profile, and its flexibility to be conformal to the objects it is attached to. Many research works have been conducted to further improve the antenna design as presented by [7, 8]. The main aims were focused on reducing the cost of the antenna, its size as well as to improve the read range and the impedance bandwidth of the tag. However, the performance of these label-type antenna are severely degraded when the tags are attached to metal objects. The shift on operating frequency, complete impedance mismatch, distorted radiation pattern were among the effects caused by the cancellation of the electrical current of the antenna by the metallic surface [9, 10]. This scenario can be best described through image theory concept. Considering that there are many RFID applications that require tag to be attached to a metal objects such as to track a metal containers and boxes in the warehouse, an antenna that is able to function properly when mounted on metal objects are required.

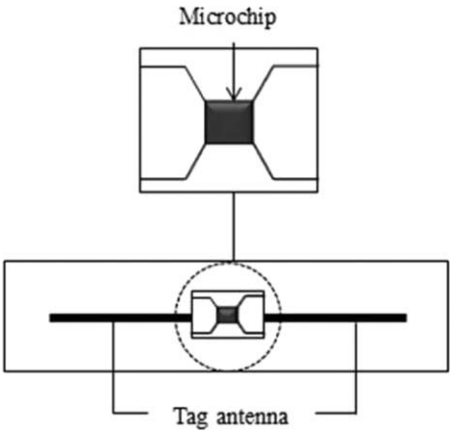

Figure 1 Typical RFID tag configuration

As a result, several type of antenna namely inverted-F antenna (IFA), planar inverted-F antenna (PIFA), and microstrip patch antenna have been proposed. These types of antennas utilize a metal plate at the bottom layer of its structure that mostly acts as a ground plane. Several works of IFA and PIFA were presented in [11, 12]. It has been experimentally proven that these antennas are able to work when mounted on metallic object. However, thick and complex structure as well as low bandwidth are the limitations of the antennas.

Microstrip patch antenna has several advantages such as low profile, robust, and easy to fabricate. A number of works have been presented to meet various requirements for RFID metallic application as presented in [13–15]. However, they have narrow bandwidth hence preventing them to be used in a global scale. The required impedance bandwidth to cater the entire UHF RFID frequency band is around 100 MHz. In addition, the structure of the antenna proposed in [16, 17] has either cross or multilayered configuration such as two substrate type, shorting plate, and wall as well as vias. To simplify the fabrication of the microstrip patch antenna, the antenna structure should use simple configuration to reduce cost. A number of studies on patch antenna without any electrical connection to the ground plate or metallic plate at the bottom layer of the antenna were successfully carried out in [18–21]. However, the drawback of these designs is the limited bandwidth for universal use.

The motivation in this research is to design a complete planar wideband microstrip patch antenna for UHF RFID tag. To match the input impedance of the proposed patch antenna to the complex impedance value of the reference microchip, Alien-Higgs 3, $Z_c = 31 - j212\,\Omega$, a rectangular loop structure is utilized. For bandwidth enhancement, two C-shaped radiating elements are inductively coupled to the rectangular loop feed to excite two resonances close to each other to form a wide impedance bandwidth. The wide bandwidth of the antenna eliminates the need to individually tuning the antenna to meet the operating frequency of specific country and region it is intended to use hence simplifying the manufacturing process. Moreover, it also ensures that the tagged items are able to be continuously tracked and monitored even when they are shipped or transferred around the world. Due to its completely planar profile, the antenna can be easily fabricated, thus providing a potential cost reduction. The rest of the article is organized as follows. Section 2 discusses the antenna design. Section 3 presents the simulation and the measurement results while conclusion is made in Section 4.

2. ANTENNA DESIGN

A planar wideband microstrip patch antenna for UHF RFID tag is proposed in this article. The antenna consists of a rectangular loop feed structure for complex impedance matching and two C-shaped radiating patches for bandwidth improvement. Unlike typical microstrip antenna where the antenna is designed to have load impedance of 50 Ω to match with the transmission line it is connected to, the input impedance of tag antenna should be designed such that it is conjugate matched with the impedance of the microchip. The performance of the complex impedance matching can be expressed in term of return loss, RL as in Eq. (1) [22]

$$\mathrm{RL} = -20\log_{10}|\Gamma| \tag{1}$$

where Γ is the voltage reflection coefficient at the antenna input terminal given by [23]

$$\Gamma = \frac{Z_{\mathrm{in}} - Z^{*}_{\mathrm{chip}}}{Z_{\mathrm{in}} + Z_{\mathrm{chip}}} \tag{2}$$

where Z_{in} is the antenna input impedance.

Due to the presence of the rectifier and energy storage capacitor inside the microchip, its impedance value is always capacitive in nature where its reactance value is large and negative. To match with the referenced microchip, a rectangular feed loop structure is chosen [24]. The feed loop acts as a transformer to transform the impedance of the patch antenna to match with the complex impedance of the microchip. The impedance seen at the antenna input impedance is given by

$$Z_{\mathrm{in}} = Z_{\mathrm{loop}} + \frac{(2\pi f M)^2}{Z_{rb}} \tag{3}$$

where Z_{loop}, M, and Z_{rb} are the input impedance of the loop, mutual inductance between the loop and the radiating element and input impedance of the radiating element. Based on Eq. (3), the input resistance, R_{in} and input reactance, X_{in} are individually expressed in Eqs. (4) and (5)

$$R_{\mathrm{in}}(f_0) = \frac{(2\pi f_0 M)^2}{R_{rb}(f_0)} \tag{4}$$

$$X_{\mathrm{in}}(f_0) = 2\pi f_0 L_{\mathrm{loop}} \tag{5}$$

Where f_0 is the operating frequency of the antenna.

Based on Eq. (6), the approximated geometry parameter of the feed loop can be calculated using Eq. (6) as shown below [25].

$$L_{\mathrm{loop}} = 0.4(a+b)\ln\left[\frac{2ab}{W_f(a+b)}\right](\mu H) \tag{6}$$

where a, b, and W_f are the perimeter of the feed loop.

This inductively coupled loop structure can be easily tuned to match with arbitrary impedance value of the microchip. The changes in loop feed parameter will mainly affect the reactance value while the input resistance is mainly determined by the distance between the loop and the radiating patches. Hence, the resistance and the reactance value at the antenna input terminal can be independently optimized which simplify the optimization process of the impedance matching. The simulation and optimization of the antenna were carried out using finite element method based software Ansoft HFSS 13.

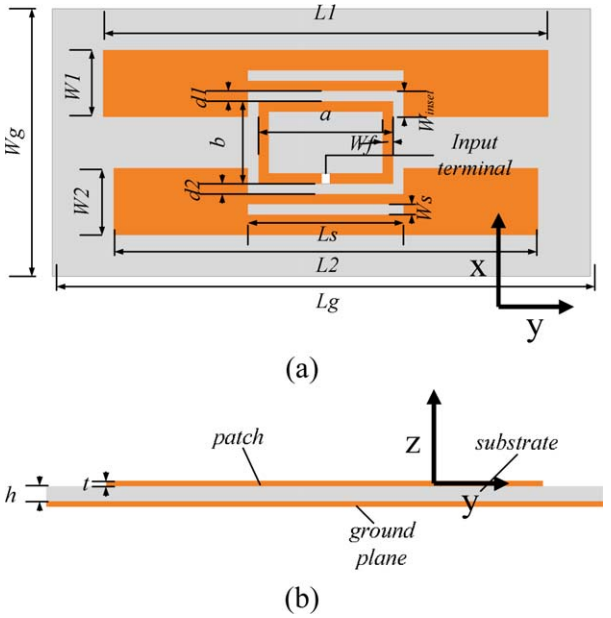

Figure 2 The geometry of the patch antenna (a) top view and (b) side view. [Color figure can be viewed in the online issue, which is available at wileyonlinelibrary.com]

To increase the impedance bandwidth of the proposed antenna, two radiating patches are used to excite two resonances close to each other to form wide impedance bandwidth to cater the entire UHF RFID band of 860–960 MHz. The initial geometry of the patches was derived from the typical rectangular patch calculated from closed form equation expressed below.

$$L = L_{\mathrm{eff}} - \Delta L \tag{7}$$

where L, L_{eff}, and ΔL are the effective length, physical length, and the extended length due to fringing field effects. ΔL is given by [26]

$$\frac{\Delta L}{h} = 0.412\frac{(\varepsilon_{\mathrm{eff}} + 0.3)\left(\frac{W}{h} + 0.264\right)}{(\varepsilon_{\mathrm{eff}} - 0.258)\left(\frac{W}{h} + 0.8\right)} \tag{8}$$

TABLE 1 Optimized Design Parameter of the Antenna

Parameter	Value (mm)
$W1$	10
$L1$	74
$W2$	10
$L2$	69
W_S	1
L_S	30
$d1$	2
$d2$	2
W_{inset}	4
t	0.0358
h	1.6
W_f	2
a	29
b	17
Ground plane and substrate	87 × 45

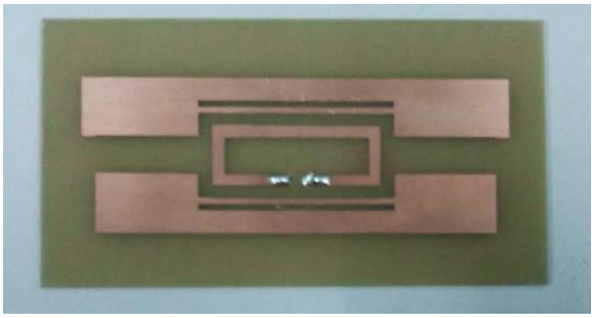

Figure 3 Prototype of the proposed wideband patch antenna. [Color figure can be viewed in the online issue, which is available at wileyonlinelibrary.com]

W is the width of the rectangular patch, h is the substrate height, and ε_{eff} is the effective dielectric constant. For the case $W/h > 1$, ε_{eff} can be calculated using Eq. (9) as follows [27]

$$\varepsilon_{\text{eff}} = \frac{\varepsilon_r + 1}{2} + \frac{\varepsilon_r - 1}{2}\left[1 + 12\frac{h}{W}\right]^{-1/2} \tag{9}$$

ε_r is the relative dielectric constant of the substrate.

The width of the radiating patches is fixed to 10 mm so as to reduce the antenna size. The substrate for the antenna is a cheap FR–4 material whose relative permittivity, ε_r, is 4.4 and the tangential loss of 0.02. The thickness of the substrate was chosen to be 1.6 mm to keep it low profile. Although a low gain is anticipated due to reduced patch width and thin dielectric substrate, it is nevertheless enough to provide a reasonable read range for the entire UHF band. To further reduce the antenna dimension, a rectangular slot is cut at one side of the patches to form a C-shaped patches. This increased the electrical current

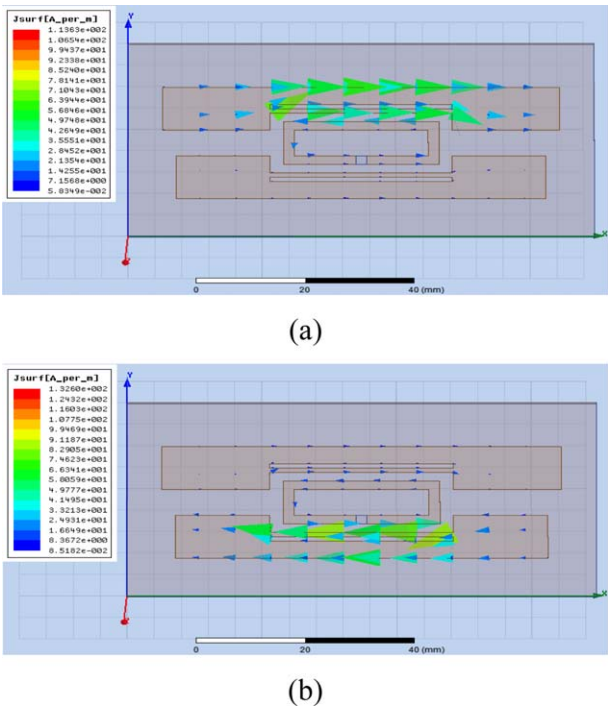

Figure 4 Surface current distribution of the antenna at two resonant modes (a) 883 MHz and (b) 953 MHz. [Color figure can be viewed in the online issue, which is available at wileyonlinelibrary.com]

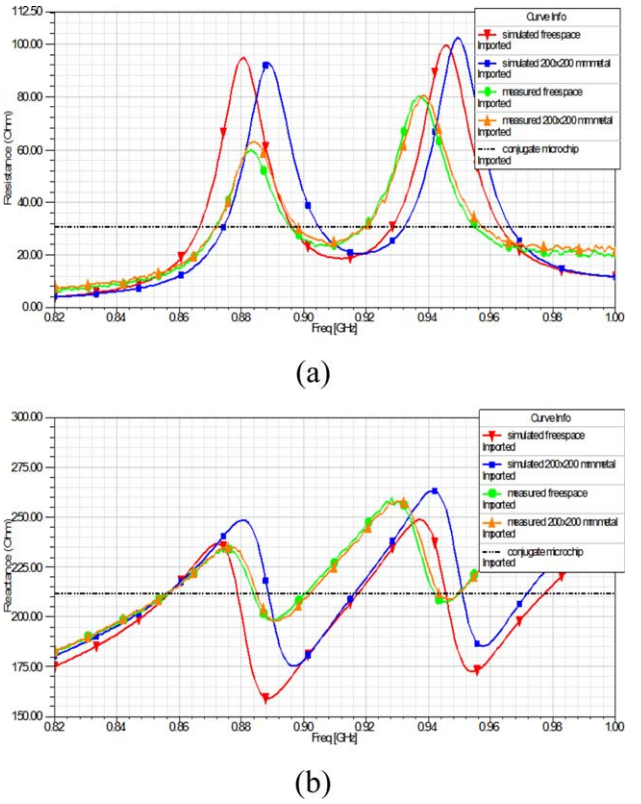

Figure 5 Simulated and measured impedance of the antenna and the microchip conjugate impedance value against frequency (a) resistance and (b) reactance value against frequency. [Color figure can be viewed in the online issue, which is available at wileyonlinelibrary.com]

length on the patches which caused the resonances to shift to lower region of frequency hence allowing the length of the patches to be reduced. Moreover, a narrow slot was embedded at each patch for easy tuning of the resonant frequency without having to change other parameter of the patches. The structure of the antenna is shown in Figure 2 and the optimized parameter value is tabulated in Table 1. The proposed metal tag antenna was then fabricated using a cheap printed circuit board technology. The prototype of the design is depicted in Figure 3.

3. RESULTS AND DISCUSSION

The surface current density of the antenna at both resonant frequencies obtained from the simulation is illustrated in Figure 4. It is clearly shown that the antenna resonates at two different

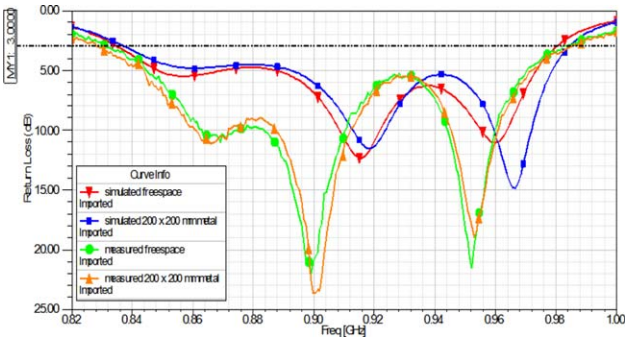

Figure 6 RL (dB) of the antenna. [Color figure can be viewed in the online issue, which is available at wileyonlinelibrary.com]

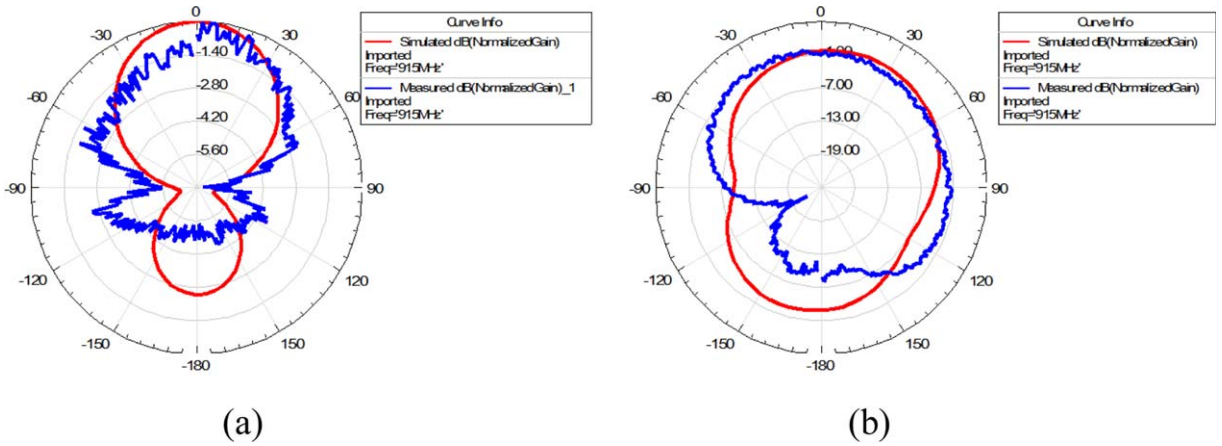

Figure 7 Simulated and measured normalized gain radiation pattern at 915 MHz. (a) *E*-plane and (b) *H*-plane field pattern. [Color figure can be viewed in the online issue, which is available at wileyonlinelibrary.com]

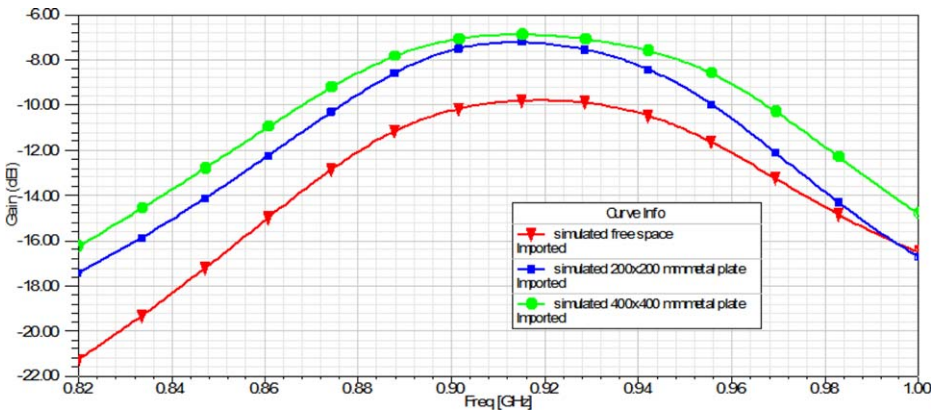

Figure 8 Simulated peak gain of the antenna. [Color figure can be viewed in the online issue, which is available at wileyonlinelibrary.com]

frequencies of 883 and 953 MHz. To investigate the functionality of the proposed antenna for tagging metallic objects, the antenna was simulated on a reference metallic plate of 200 × 200 mm^2. Furthermore, the measurement of the antenna input impedance was carried out on two scenario, on free space and when being mounted on metallic plate.

The simulated and measured impedance of the antenna for the two scenarios are depicted in Figure 5. A good agreement between the two results proves that good impedance matching is realized throughout the entire UHF frequency band. The slight different in input resistance between the simulation and measurement results are due to fabrication inaccuracies and the surrounding effects during the measurement process. Although a shift in resonances was observed between the two scenarios from the simulation, however measurement results show that there was hardly any shift in frequency between them. This proves that the antenna is able to function properly when being mounted on metal objects when most label-type tag antennas fail to work. In addition, the half-power impedance bandwidths (RL $\geq$ 3 dB) for both cases are well above the required 100 MHz bandwidth as shown in Figure 6.

The simulated and measured normalized gain radiation patterns of the antenna at the operating frequency of 915 MHZ are shown in Figure 7. Both radiation patterns show good agreement between them. Furthermore, the simulated peak gain of the antenna is illustrated in Figure 8. It is observed that the gain of the antenna increased when being attached to a larger metal plate. This shows that the performance of the proposed patch antenna will improve when use for metallic application.

4. CONCLUSION

A planar wideband microstrip patch antenna is proposed in this research. Two C-shaped patches are fed by rectangular loop feeding structure to increase the bandwidth of the antenna for universal usage. The planar structure of the antenna provides ease of fabrication due to the exclusion of multi and cross layered configuration. The design of the antenna is supplemented by simulation and experimental results. The simulated and measured half-power bandwidths of the antenna (RL $\geq$ 3 dB) are 159 and 155 MHz, respectively. Moreover, the peak gain of the antenna is sufficient to give reasonable read range for the entire UHF frequency band. In the future, measurement for the read range of the proposed tag antenna will be carried out.

REFERENCES

1. W. Lorchirachoonkul and J. Mo, Virtualisation of RFID supply chain. In: 5th International Conference on Intelligent Sensors, Sensor Networks and Information Processing (ISSNIP), Melbourne, VIC, 2009.

2. J. Liu et al., Dual frequency based Real Time Location System using passive UHF RFID. In: IEEE 9th International Conference on ASIC (ASICON), Xiamen, China, 2011.
3. K. Finkenzeller, RFID handbook, 2nd ed., Wiley, West Sussex, 2003.
4. G. Marrocco, The art of UHF RFID antenna design: Impedance-matching and size-reduction techniques, IEEE Antennas Propag Mag 50 (2008), 66–79.
5. D.M. Dobkin, The RF in RFID: Passive UHF RFID in practice, Elsevier Inc., Massachusetts, 2008.
6. Regulatory status for using RFID in the UHF spectrum 28 September 2012. Available at: http://www.gs1.org/docs/epcglobal/UHF_Regulations.pdf, accessed on October 10, 2012.
7. G. Monti et al., Broad-band dipole for RFID applications, Prog Electromagn Res C 12 (2010), 163–172.
8. X. Zhou and G.Q. Luo, A broadband and miniaturized UHF RFID tag antenna with T-matching network. In: Microwave Workshop Series on Millimeter Wave Wireless Technology and Applications (IMWS), Nanjing, China, 2012.
9. N. Ghannay et al., Effects of metal plate to RFID tag antenna parameters. In: Microwave Symposium Mediterrannean (MMS), Tangiers, 2009.
10. L.-F. Mo et al., Analysis of dipole-like ultra high frequency RFID tags close to metallic surfaces, J Zhejiang Univ Sci A 10 (2009), 1217–1222.
11. J. Xi et al., Platform-tolerant PIFA-type UHF RFID tag antenna. In: IEEE International Conference on RFID, Orlando, FL, 2010.
12. L. Mo and C. Qin, Tunable compact UHF RFID metal tag based on CPW open stub feed PIFA antenna, Int J Antennas Propag 2012 (2012), 8.
13. J. Yan et al., A novel patch antenna for UHF band RFID tag. In: 7th International Conference On Wireless And Optical Communications Networks (WOCN), 2010.
14. H.-W. Son and S.-H. Jeong, Wideband RFID tag antenna for metallic surfaces using proximity-coupled feed, IEEE Antennas Wireless Propag Lett 10 (2011), 377–380.
15. L. Mo and C. Qin, Planar UHF RFID tag antenna with open stub feed for metallic objects, IEEE Antennas Propag Mag 58 (2010), 3037–3043.
16. J.Z. Huang et al., A compact broadband patch antenna for UHF RFID tags. In: Asia Pacific Microwave Conference (APMC), Singapore, 2009.
17. J.-H. Lu and K.-T. Hung, Planar UHF RFID tag antenna with bandwidth enhancement. In: Cross Strait Quad-Regional Radio Science and Wireless Technology Conference (CSQRWC), Harbin, 2011.
18. M. Eunni et al., A novel planar microstrip antenna design for UHF RFID, J Syst Cybern Inf 5 (2007), 6–10.
19. J. Dacuña and R. Pous, Low-profile patch antenna for RF identification applications, IEEE Trans Microwave Theory Tech 57 (2009), 1406–1410.
20. H.-G. Cho et al., Design of an embedded-feed type microstrip patch antenna for UHF radio frequency identification tag on metallic objects, IET Microwaves Antennas Propag 4 (2010), 1232–1239.
21. T. Tashi et al., A complete planner design of microstrip patch antenna for a passive UHF RFID tag. In: 17th International Conference on Automation and Computing (ICAC), 2011.
22. T.S. Bird, Definition and misuse of return loss, IEEE Antennas Propag Mag 51 (2009), 166–167.
23. C.-H. Loo et al., Chip impedance matching for UHF RFID tag antenna design, Prog Electromagn Res 81 (2008), 359–370.
24. H.-W. Son and C.-S. Pyo, Design of RFID tag antennas using an inductively coupled feed, Electron Lett 41 (2005), 994–996.
25. P.H. Yang et al., Compact metallic RFID tag antennas with a loop-fed method, IEEE Trans Antennas Propag 59 (2011), 4454–4462.
26. C.A. Balanis, Antenna theory analysis and design, 3rd ed., John Wiley and Sons, New Jersey, 2005.
27. G. Kumar and K.P. Ray, Broadband microstrip antenna, Artech House, Noorwood, MA, 2003.

© 2014 Wiley Periodicals, Inc.

CONSCIOUSNESS AND SUBCONSCIOUSNESS DETECTION MODEL UNDER ČERENKOV RADIATION

P. P. Yupapin,[1] N. Thammawongsa,[2] and J. Ali[3]
[1] Department of Physics, Advanced Studies Center, Faculty of Science,
[2] King Mongkut's Institute of Technology Ladkrabang, Bangkok 10520, Thailand
[3] Department of Electronics, Faculty of Technology, Udon Thani Rajabhat University, Udon Thani 42000, Thailand; Corresponding author: kypreech@kmitl.ac.th
[4] Department of Physics, Universiti Teknologi Malaysia, Johor Bahru 81300, Malaysia

Received 8 November 2013

ABSTRACT: *A new model of space-time paradox concept is proposed to describe the <consciousness|subconsciousness> states, where the connection between whispering gallery mode probe and brain signal form and the mind-mater interfacing information can be described. The uncertainty of the paradox pair is described by using the well known Heisenberg's uncertainty principle. This proposal is useful for possible mind and dream investigations.* © 2014 Wiley Periodicals, Inc. Microwave Opt Technol Lett 56:1584–1587, 2014; View this article online at wileyonlinelibrary.com. DOI 10.1002/mop.28388

Key words: *Čerenkov radiation; subtle energy; space-time paradox; enlightenment; extrasensory perception*

1. INTRODUCTION

Natural phenomenon is basically localized by a couple (pair) and defined by the orthogonal state of the possible outcomes, which is an early and influential critique leveled against quantum mechanics. Albert Einstein and his colleagues Boris Podolsky and Nathan Rosen designed a thought experiment intended to reveal what they believed to be inadequacies of quantum mechanics known as EPR paradox. To that end, they hypothesized a consequence of quantum mechanics that its supporters had not noticed but looked unreasonable at the time [1]. The routine explanation of this effect was, at that time, provided by Heisenberg's uncertainty principle. Physical quantities come in pairs which are called conjugate quantities. Examples of such conjugate pairs are position and momentum of a particle and components of spin measured around different axes. When one quantity is measured, and became determined, the conjugated quantity became indeterminate. Heisenberg explained this as a disturbance caused by measurement. The other pairs of EPRs can be categorized by the followings such as Particle-Antiparticle: **<P|A>**; Dark|Bright soliton pair:**<D|B>** [2];Entangled photon:**<0|1>**; polarization: <H|V>; Consciousness|Subconsciousness: **<C|SC>**; and Čerenkov radiation: **<S|T>**, where few of them have been proposed.

1.1. Čerenkov Radiation

Two states of radiation can be occurred only one state in each appearance, so we use the terms of space-time paradox for the two states as **<S|T>**. Čerenkov radiation is the electromagnetic radiation, which is emitted when a charged particle (such as an electron) passes through a dielectric medium at a speed greater than the phase velocity of light in that medium. The charged particles polarize the molecules of that medium, which then turn back rapidly to their ground state, emitting radiation in the process [3]. Čerenkov luminescence imaging is an emerging optical preclinical modality based on the detection of Čerenkov